

**Overland flow depth- velocity and infiltration rate at desert conditions
(Patagonian Monte): field plot results and model.**

M. J. Rossi¹ and J.O. Ares¹

5 [1]{National Patagonic Centre, CONICET, Blvd. Brown 2915, 9120 Puerto Madryn,
Chubut, Argentina}

Correspondence to: M.J. Rossi (rossijulieta@gmail.com). TE-FAX: 54 280 4451024.

National Patagonic Centre, CONICET, Blvd. Brown 2915, 9120 Puerto Madryn, Chubut,
Argentina

10

J. O. Ares: joares@gmail.com

Abstract

Water infiltration and overland flow are relevant in considering water partition among plant life forms, the sustainability of vegetation and the design of sustainable hydrological models and management. In arid and semi-arid regions these processes present characteristic trends imposed by the prevailing physical conditions of the upper soil as evolved under water-limited climate. A set of plot-scale field experiments at the semi-arid Patagonian Monte (Argentina) was performed in order to estimate infiltration-overland flow parameters. The micro-relief of undisturbed field plots was characterized at z-scale 1 mm through close-range stereo-photogrammetry and geo-statistical tools. The overland flow areas produced by controlled water inflows were video-recorded and the flow velocities were measured with image processing software. Antecedent and post-inflow moisture were measured, and texture, bulk density and physical properties of the soil at the upper vadose zone were estimated based on soil core analyses. Field data were used to calibrate a physically-based, time explicit model of water balance in the upper soil and overland flows with modified Green-Ampt (infiltration) and Chezy (overland flow) algorithms. Modelling results satisfy validation criteria based on the observed flow areas and velocities, water mass balance of the upper vadose zone, infiltration depth, slope along run-off plume direction, and depression storage areas. Results indicate that overland flow velocities and infiltration-overland flow mass balances are consistently modelled by considering variable infiltration rates corresponding to depression storage and/or non-ponded areas. Estimates of hydrodynamic parameters of overland flow (Chezy frictional C , Darcy-Weisbach f , average overland flow depth, Reynolds-Froude numbers, flow velocity) are informed. To our knowledge, the study here presented is novel in combining several aspects that previous studies do not address simultaneously: 1. Overland flow and infiltration parameters were obtained in undisturbed field conditions; 2. Field measurements were coupled to a physically based model of the expansion of overland plumes and depth of soil moisture, without interfering effects of simultaneous rainfall; 3. The effect of depression storage areas in infiltration rates and depth-velocity of overland flows is highlighted. Relevance of the results to other similar desert areas is supported by the accompanying biogeography analysis of similarity of the environment where this study was performed with other desert areas of the world.

Keywords: Desert Hydrology, Infiltration, Overland flow, Depression Storage, Patagonia.

1 Introduction

The complexity of interactions between overland flow and infiltration has long received attention in hydrological studies. The spatial variability of soil microtopography has been identified as a major determinant of infiltration rates and the hydrological response of watersheds (Abrahams et al., 1990; Köhne et al., 2009; Darboux et al., 2001). Usual procedures to study run-off-infiltration processes involve the use of hydrological models based on hydrograph records. Although a large body of literature has been devoted to the criteria used to inspect hydrograph records (Ewen, 2011) less attention has been paid to the fact that many hydrological models that can accurately reproduce hydrograph records, produce severely biased estimates of overland flow velocities (Mügler et al., 2011; Legout et al., 2012) or Reynolds-Froude numbers (Tatard et al., 2008).

Infiltration-run-off models need to calculate the overland flow velocity and depth to be able to simulate the flow of water over the land surface. Frictional effects must be accounted for, usually through simplifying equations of the fundamental hydrodynamic laws on continuity and momentum balance involved. To this aim, most field and laboratory studies on overland flow use the Darcy-Weisbach's f and Manning's n (Darboux et al., 2001; Hessel et al., 2003; Li, 2009). Both of these are calculated from the same variables (flow rate, terrain slope, roughness, Reynolds numbers) and both suffer from limitations imposed by the high variability of the represented effects both in space and time. Abrahams et al. (1990) studied Darcy-Weisbach's f for desert hill slopes and found that it varies with the rate of flow. Since the rate of flow is highly variable in space, so too is f . Analogous limitations can be expected in relation to Manning's n .

In the case of arid and semi-arid areas, complex interactions between run-off generation, transmission and re-infiltration over short temporal scales (Li et al., 2011; Reaney, 2008) add difficulties in the estimation of infiltration-overland flows. In these areas, the soil surface is predominantly flat and gently sloped at extended spatial scales, and the excess rainfall moves at the surface of the soil in very shallow structures combining small overland flow areas interspersed with finely ramified fingering patterns of small channels. Infiltration in arid and semi-arid regions can also be modified by the development of water-repellent areas (Lipsius and Mooney, 2006) which in cases occur in relation to soil microtopography (Biemelt et al., 2005).

Composite patterns of overland flow (Parsons and Wainwright, 2006; Smith et al., 2011) can be expected to produce spatially heterogeneous patterns of water infiltration in the upper soil (van Schaik, 2009). Results obtained by Esteves et al. (2000) in laboratory run-off plots, indicate that despite the soil being represented by only one set of parameters, infiltration was not homogeneous all over the plot surfaces. They concluded that the microtopography had a strong effect on observed flow directions, producing small ponds along the paths of flow and altering the flow depths and velocity fields. Similar flow distributions were observed by Parsons et al. (1990) in plots under semi-arid conditions. They advanced two explanations for the observed distributions. First, following the application of Darcy's law the infiltration is an increasing function of the applied water depth at the soil surface. Secondly, the water available (supply rate) to satisfy the infiltration is greater on run-off preferential paths.

Descroix et al. (2007) observed that catchments and small plot studies in arid regions usually show a so-called "hortonian" trend, with characteristic absence of base flow. This was the case in semi-arid northern Mexico for catchments as large as tens of thousands km², and for approximately 500 km² in the Western Sierra Madre. Latron and Gallart (2007) working at the Pyrenees determined that there is a strong relationship between the base flow and the extension of saturated areas at the basin scale. In Australia's semi-arid rangelands, patches of bare soils were determined to be the main run-off controlling factor (Cammaraat 2002, Bartley et al., 2006).

Thompson et al. (2011) observed that the lateral redistribution of ponded water generated during intense rainstorms plays an important role in the hydrological, biogeochemical and ecological functioning of patchy arid ecosystems. Lateral redistribution of surface water in patchy arid ecosystems has been hypothesized to contribute to the maintenance of vegetation patches through the provision of a water subsidy from bare sites to vegetated sites (Bromley et al., 1997). Such infiltration-overland flow processes occur during hortonian run-off events on sloping ground. Surface flow redistribution may also occur on flat ground if the presence of vegetation patches creates contrasts in infiltration rate between dry soil and water saturated areas. Changes in the pattern of surface water re-distribution occur during early stages of desertification (Ares et al., 2003). Several studies indicate that the horizontal movements of the naturally scarce rainfall water on the surface soil in arid regimes contribute to define the spatial pattern of woody and herbaceous vegetation forms as well as the extent of bare soil patches (Aguiar and Sala, 1999; Ares et al., 2003; Borgogno et

al., 2009; Dunkerley, 2002).

Water infiltration in the soil has been successfully modelled through various techniques. Some existing models apply numerical solutions to the Richards equation (Radcliffe and Simunek, 2010; Weill et al., 2011) while others use various modifications to the Green-Ampt (Green and Ampt, 1911) model (Gowdish and Muñoz Cárpena, 2009; Mengistu et al. 2012; Schröder, 2000). A strong control on field-scale infiltration is exerted by the horizontal spatial variability of infiltration properties (Lipsius and Mooney, 2006; van Schaik, 2009).

Experiments and models on overland flow have extensively used so-called kinematic wave- reduced solutions to the Saint-Venant (S-V) equations (Mügler et al., 2011; Thompson et. al., 2011). The numerical solutions of these reductions require the estimation of frictional effects acting on overland flow. Also, in order to construct continuity equations, the average depth of the overland flow must be known as well as its propagation velocity. Although the S-V equations have consistently proved capable of accurately simulating hydrographs at plot scale, most of the assumptions underlying the estimation of frictional forces and flow depth do not hold when applied to overland flows in field conditions (Smith et al., 2007). Moreover, the choice of roughness models to be used in the S-V equations is most often done in the purpose of increasing the hydrograph quality, while the actual travel time of water is ignored. In extended hydrological practice, frictional factors are usually taken from published tables or assumed spatially constant (Esteves et al., 2000).

Plot experimentation has long been relevant in developing physically based models of water flow (Köhne et al., 2009). The term usually refers to laboratory (Antoine et al., 2011; Dunkerley, 2001, 2002; Legout et al. 2012) or field (Esteves et al., 2000; Mengitsu et al., 2012) studies involving areas in the scale of some few square meters, where water flow conditions can be manipulated with varying success. Plot experiments are often used to obtain estimates of depression storage (DS) (Antoine et al., 2011) in studies of overland flow, in the context of interpreting DS retention effect on hydrograph records (Govers et al., 2000; Hansen, 2000, Darboux et al. 2001). The underlying concept is that DS areas behave as a temporary passive storage of overland flow resulting in a delay in the hydrograph signals. This in turn prompts interest in its direct measurement at the plot scale through geometrical analysis of elevation models (Planchon and Darboux, 2002) or from surface roughness measurements (Antoine et al., 2011).

This study is part of a larger project at the National Patagonic Centre (Chubut, Argentina) to develop tools for the eco-hydrological analysis of desertification processes. It builds on previous results obtained by Ares et al. (2003) indicating that early desertification processes involve modifications of the overland flow patterns and its distribution among the various vegetation life forms in the Patagonian Monte (Argentina). Here, an experimental protocol of field plot experiments and coupled simulation model to estimate infiltration and overland flow parameters in the Monte environment is presented. The protocol involves parameters that can be quantitatively estimated with an adequate degree of precision (overland flow velocity, infiltration depth, soil water content, depression storage area) as well as others that can indirectly be estimated (surface frictional effect, average overland flow depth, Reynolds-Froude numbers). Specifically, this study addresses: (1) the effect of plot microtopography on the infiltration-overland flow, (2) the estimation of parameters (flow velocity, depth, friction, infiltration rate) needed to calculate water movement at the soil surface. A biogeography analysis of the similarity of the experimental site in this study with other areas of the world is also included to ease eventual pertinent comparisons of the results here presented with those obtained in similar studies.

2 Site and field experiments

2.1 Biogeography of the experimental site

The Monte desert is a South American subtropical to warm temperate desert and semi-desert located in western Argentina from 24°15'S to 44°20'S. The study here presented was performed at a representative site of the biome in the area of the Patagonian Monte, a temperate region with a Mediterranean-like rainfall regime produced by the westerlies from the Pacific affected by the rain shadow effect from the Andes (Abraham et al., 2009). Past precipitation records, observed (Haylock et al. 2006) and predicted precipitation anomalies expected under various scenarios of climate change (Carrera et al., 2007) indicate that precipitation events may occur at both high (> 20 mm/day) as well as low (< 3 mm/day) depths. This pattern corresponds to alternative atmospheric mechanisms of rain generation characteristic of the tropical regime prevailing at the northern part of the territory or prevailing winter-rain of the temperate latitudes (Prohaska, 1976). Both types are observable at times along most of the area occupied by the biome. There is a remarkable convergence between the desert areas of North and South America (Monte, Chihuahuan-Sonoran deserts)

consisting in the same climate subtypes, the same dominant vegetation and the same combination of biological forms (Morello, 1984 as quoted by Abraham et al., loc. cit.). Similar conditions are extensively found in arid and semi-arid climates worldwide (Mares et al., 1985).

5 This study was carried out at the wildlife refuge "La Esperanza", (southern portion of the Monte desert) which occupies an area of about 42000 km² in south-eastern Argentina (León et al., 1998; Soriano, 1950). The mean annual temperature is 13.4° C and the mean annual precipitation is 235.9 mm (1982–2001). The characteristics of the site as
10 representative of the Monte desert are based on the analysis of the dominant vegetation life forms. The local vegetation covers about 40% and 60% of the soil in a random patchy structure with three vegetation layers: the upper layer (1–2 m height) dominated by tall shrubs (*Larrea divaricata*, *Schinus johnstonii* Barkley, *Chuquiraga erinacea* Don., *Atriplex lampa* Gill. ex Moq., and *Lycium chilense* Miers ex Bert.), the intermediate layer (0.5–1.2 m height) also composed by dwarf shrubs (*Nassauvia fuegiana* (Speg.) Cabrera, *Junellia seriphioides* (Gillies and Hook) Mold., and *Acantholippia seriphioides* (A. Gray) Mold.), and
15 the low layer (0.1–0.5 m height) dominated by perennial grasses (*Nassella tenuis* (Phil.) Barkworth, *Pappostipa speciosa* (Trin. and Rupr.) Romasch, and *Poa ligularis* (Nees ex Steud) (Ares et al., 1990; Carrera et al., 2008). Soils are a complex of Typic Petrocalcids–Typic Haplocalcids with a fractured calcium carbonate layer from 0.45 to 1 m below the soil
20 surface (del Valle, 1998). Upper soil texture types (USDA) are sandy or loamy sand.

2.2 Field experiments

Ten field plot experiments in undisturbed bare soil patches (800×800 mm) along a down-sloping transect (103 to 64 m.a.s.l.) from S: -42.17046, W: -64.96343 to S: -42.21366,
25 W: -64.99225 were conducted during the dry season on days with air temperatures in the range 20–32° C. The spatial arrangement of plots was aimed to explore an altitudinal range of variation of soil texture. Water inflow to plots was achieved through a portable, wind protected, single-nozzle system mounted at 30 cm above soil level on a wooden frame and calibrated with a pressure gauge to supply water inflow rates in the range 225–4500 mm³/s to
30 a small area (4.7 ± 5.2%) of each plot that was further neglected for estimations of overland flow velocities. This created two plot sub-regions: one directly receiving the water inflow and another receiving the overland flow resulting from the excess of water input to the

former. The water inflow range was aimed at simulating extreme flow accumulation values of modal low-high daily rain depths in the area (see Section 2.1). Flow accumulation was estimated with a flow routing algorithm (Tarboton and Ames, 2001). The frame supported a Kodak EasyShare Z712 IS 7.1 MP camera (© Eastman Kodak Company, Rochester, New York) with video mode, at near zenith position over the centre of the plot and about 1 m above ground level to obtain images of the whole plot area. Video records of the expanding overland wetted areas were obtained during experiments of varying time length (72-1128 s) until the wet front reached some of the borders of the camera image in any direction. This implied a zero-discharge condition (all overland flow was infiltrated in the wetted area at the end of the experiments).

Soil moisture was evaluated immediately after the water inflow ceased with a TDR (Time-Domain Reflect meter, TRIME®-FM, Ettlingen) pin (50 mm) probe inserted at a proper angle in order to sample the top 30 mm of the soil at equidistant (30-35 mm) points of a grid covering the whole overland flow area and neighbouring dry points. TDR estimates of soil moisture were calibrated with gravimetric estimates obtained by extracting 2-5 soil cores (\varnothing : 40 mm) along the main axes of the overland flow plume, (at the centre of the directly wetted area and equidistant positions up to the wetted border and control at nearby dry soil, Figure 1a). Soil cores were extended to depths 0-30, 30-90 and 90-180 mm, brought to the laboratory in sealed containers and wet-dry (105 °C) analysed for moisture content. Gravimetric moisture was expressed in volumetric terms through correction with soil bulk density measured through the excavation method (ISO 11272, 1998) at a nearby location. Maps of soil moisture in the wetted area at the end of the water inflow period were based on calibrated TDR estimates ($y = 1.166x + 0.05$; $R^2 = 0.92$, $n = 101$; x : gravimetric θ estimate). Map values were obtained by interpolation of 4-6 closest TDR estimates, based on a specified search radius algorithm (Idrisi v. 14.02, Clark Labs, Worcester).

The texture of the extracted soil core samples was measured with Lamotte's 1067 texture kit (LaMotte Co., Chestertown) calibrated with replicate estimates obtained at two reference laboratories (National Patagonic Centre, National University of the South, Argentina) with the Robinson's protocol (Gee and Bauder, 1986). Parameters corresponding to residual volumetric moisture (θ_r), saturated moisture content (θ_s), saturated hydraulic conductivity (K_{sat}) tortuosity-connectivity (L), and shape of the soil moisture-water head function ($\log_{10}\alpha$, $\log_{10}n$) (Van Genuchten, 1980) corresponding to the obtained soil samples were estimated based on textural data through an ANN (Artificial Neural Net) pedotransfer

algorithm (Rosetta v. 1.2, US Salinity Laboratory, Riverside) developed by Schaap and Leij (1998).

A methodology (Rossi and Ares, 2012) combining Close-Range Stereophotogrammetry (CRS) and Geo-Statistical Modelling (GSM) was applied to obtain Digital Elevation Models (DEM) (resolution 8.23 ± 0.24 mm, $P < 0.05$, $n = 10$). The coordinates of 9 control points and a minimum of 64 targets obtained through CRS were loaded to an application (I-Witness v. 1.4, DCS Inc., Bellevue, WA, USA) for ortho-rectification and further processed with a kriging algorithm (Surfer v. 7, Golden Software Inc., Colorado) to obtain plot DEMs and DEM-based flow vector fields. At one control plot, the DEM obtained with the CRS-GSM procedure was further compared with another obtained through a regular optical level (Kern GK1-AC, D'iberville, MS) /staff method, using the same control points for both procedures, with the optical level installed close (3m) to the staff with mm intervals, in order to minimize reading error. Digital video-images of the overland flowing water plume were selected at regularly spaced time intervals (6-240 s). The spacing of time intervals within this range was selected according to the duration of the experiments. Time intervals were constant ($T_i = 6$ s) for those experiments with high water input rates of short duration (Plots 1 to 4). In longer experiments with low water input rates (Plots 5 to 10), time intervals (s) were selected according to $T_i = (e^{(0.265 \times ts)}) \times 6$, where ts is the cardinal number of the interval. This resulted in short intervals between images during the early stages of fast overland flow and gradually longer intervals during later stages of slow overland flow. Images were then exported to an image processing application (Idrisi v. 14.02, Clark Labs, Worcester), ortho-rectified (RMSE: 7.59 ± 1.3 mm, $P < 0.05$, $n = 10$) and overlaid to their corresponding plot DEM and map of flow vector fields at the same resolution of the DEM. Flow vectors were estimated from the DEM. At any map node flows were in the direction of the steepest descent and the magnitude of the arrow depended on the steepness of the descent. The terrain height change corresponding to the overland flow advance at each time interval was evaluated by averaging the altitude differences between all pixels along the borders of successive images. Depression storage (DS) (Antoine et al., 2011) areas were identified at each time interval by measuring the area advanced by the overland plume during the interval, discriminating between: 1. Area advanced down slope, and 2. Area advanced in direction opposed to the expected gravity flow. The fraction of the area of the plume where depression

storage occurred within the wet plume area was then estimated through the ratio of areas 2/(1+2) above mentioned (Figure 1b).

3 Model

The changes observed at the overland flow areas and subsurface soil water content at the plots during the experiments were modelled with a physically based continuity model consisting in a set of non-linear ordinary differential and continuity equations with time variable parameters, each representing the storage of overland water and at the upper vadose zone, respectively:

$$\frac{dQ_o}{dt} = W - IN(t) - O(t) \quad (1)$$

$$\frac{dQ_v}{dt} = IN(t) \quad (2)$$

$$CW = Q_o + Q_v \quad (3)$$

Q_o : Water stored at the overland plume (mm³).

Q_v : Water stored at the upper vadose zone (mm³).

W : Water inflow (mm³/s).

$IN(t)$: Total infiltration flow (mm³/s).

CW : Cumulative water inflow (mm³).

$O(t)$: overland flow (mm³/s).

Note that evaporation was disregarded due to the short duration of the field experiments. While W is time-constant for each single plot experiment, $IN_t - O_t$ can be expected to change with time depending on the effects of soil micro-relief and the physical properties of the surface soil. Further, the overland flow plume contains storage areas where free water accumulates during the water inflow period, and other parts where the water inflow is not enough to maintain free water at the soil surface. Accordingly, $IN(t)$ may be expected to result from the composition of flows under both saturated and unsaturated conditions. Saturated conditions occur at DS areas, while both saturated and/or unsaturated

infiltration flows can occur at other areas depending on their water content:

$$IN(t) = IN_{sat}(t) + IN_{unsat}(t) \quad (4)$$

$IN_{sat}(t)$: transient, saturated infiltration flow from DS areas (mm^3/s).

5 $IN_{unsat}(t)$: transient, saturated and/or non-saturated infiltration flow from non-DS areas (mm^3/s).

The IN_{sat} flow was modelled through a Green-Ampt's concept (Green and Ampt 1911; Muñoz-Cárpena and Gowdisha, 2005) where infiltration was assumed to occur under saturated conditions depending on the gradient of water head between the soil surface and a point at the infiltrating wetting front:

$$IN_{sat} = K_s \times \left[\Psi_f \times \left(\frac{\theta_s - \theta(t)}{F} \right) + 1 \right] \times A_{DS} \quad (5)$$

$$F = z_f(t) \times (\theta_s - \theta(t)) \quad (6)$$

K_s : saturated hydraulic conductivity (mm/s).

15 $\psi_f(\theta)$: suction at the wetting front (mm).

$\theta_s, \theta(t)$: saturation and instantaneous volumetric water content at the wetting front respectively (dimensionless).

F : accumulated infiltration (mm).

A_{DS} : DS area (mm^2).

20 $z_f(t)$: instantaneous water infiltration depth (mm).

In areas of the overland plume where no DS occurs, water infiltration was assumed to occur under unsaturated conditions. This component of the infiltration flow was estimated by replacing in Eq. (5, 6) through corresponding terms:

$$IN_{unsat}(t) = K_h(\theta(t)) \times \left[\Psi_f(\theta(t)) \times \left(\frac{\theta(t) - \theta_i}{F} \right) + 1 \right] \times (A(t) - A_{DS}) \quad (7)$$

$K_h(\theta(t))$: variable hydraulic conductivity (mm/s).

θ_i : Antecedent water content of the soil.

$A(t)$: Wet area of overland plume at time t (mm²).

$K_h(\theta(t))$ and $\psi_f(\theta(t))$ were estimated through the solution (van Genuchten, 1980) of Mualem's (Mualem, 1976) formulation to predict the relative hydraulic conductivity from knowledge of the soil-water retention curve.

The instantaneous overland water volume was estimated as:

$$Q_o = A(t) \times d(t) \quad (8)$$

$d(t)$: average depth of the overland flowing water volume at time t (mm).

flowing in the x - y space, with varying velocity depending on the local altitude gradient along its border, such that $d(t)$ is inversely related to the slope of the underlying soil surface. This relation would follow Darcy's general form of frictional law (Dingman, 2007; Mgler et al., 2011):

$$d(t) = \left(\frac{W}{C} \right)^2 / S(t, t+dt) \quad (9)$$

C : Proportionality constant.

$S(t, t+dt)$: Average terrain height drop around the overland plume during the interval $t, t+dt$ (mm).

where the Darcy's velocity term is replaced in this case with the water inflow rate W , and $S(t, t+dt)$ was obtained from successive video images of the overland flow overlaid on the plot DEMs. The frictional term C was found through inverse modelling of the continuity Eqs. (1)-(3), solved through numerical integration with a fourth-order Runge-Kutta approximation, at solution time intervals $0.06 \leq \Delta t \leq 0.3$ s, and an accepted mass balance error $e \leq 1 \times 10^{-7}$ mm³.

3.1 Modelling parameters and variables: convergence and validation

Table 1 summarizes the parameters and variables measured and modelled in relation with the field plot experiments. Model estimates were inspected both at the plot and inter-plot scales for multiple convergence to all measured values describing the experimental setting, the morphology of the plot surface soil and the hydrological properties of the upper vadose zone.

- 5 The criteria at intra-plot scale in the case of parameters 1-8 was strict convergence to measured data values which were used as model input. Convergence to parameter 9 (K_s) was required within the confidence interval of the ANN estimation process as reported in Shaap and Leij (1998). Variable 10 ($A(t)$) was required to converge to data as estimated through a Nash-Sutcliffe's Efficiency Coefficient ($EC \geq 0.99$) (Nash and Sutcliffe, 1970). Values of
10 11-16 were required to converge to:

$$\sum_{i=1, n} (x_i - x_{data})^2 = \min \quad (10)$$

where x_i is the model estimate and x_{data} is the corresponding experimental-measured value.

- 15 11-16 were further tested for convergence to data at the inter-plot scale such that their correlation with measured values would be significant at $P < 0.001$ over the set of 10 plots studied. Variables 12-14 are average values of the corresponding variable over the simulation time.

- Several procedures were used for model validation. Unit consistency and ranges of
20 K_s , $K_h(\theta(t))$, $\psi_f(\theta(t))$, were independently checked through comparison with estimates obtained with CHEMFLO-2000 (Nofziger and Wu, 2003), an application that solves Richards equations in one-dimension to simulate transient water (and chemical) transport in soils. CHEMFLO-2000 solves the Richards equation in one dimension ($-z$); accordingly, comparisons with this model were limited to data corresponding to the soil core extracted at
25 the water inflow area. Confidence intervals ($P < 0.05$) of the correlation coefficient r of measured-modelled values 9-16 were built by bootstrapping paired comparisons such that randomly selected five plots were used for model calibration and the rest for model validation. z_f and θ_{end} values observed in the field were additionally tested for consistency with CHEMFLO-2000 estimates.

- 30 Additionally, the following variables were defined based on model outputs:

$$\sigma_S = (\sum_{t=1, n-1} (S(t) - S^*)^2 / (n-1))^{0.5}, \quad (11)$$

S^* : $S(t)$ average at the end of the water inflow period (mm).

the standard deviation of $S(t)$, as a measure of soil surface roughness independent of plot slope effects.

$$5 \quad \gamma_{A/CW} = a - b / (A^* / CW)^{0.5}, \quad (12)$$

$\gamma_{A/CW}$: exponential ratio of the total wet surface soil area A^* to the accumulated water inflow volume at the end of the water inflow period (mm^{-1}); $a = 2.42E-04$; $b = 3.31E-04$)

as a measure of the plot capacity to retain water inflow.

$$\varsigma = \int_0^n (O(t) / \frac{dQ_v}{dt}) dt \quad (13)$$

10 ς : run-off coefficient

where ς is a time-integrated (dimensionless) run-off estimate, including transient depression storage.

$$d^* = (\sum_{t=1, n} d(t)) / n \quad (14)$$

d^* : mean $d(t)$ (mm) at the end of the $t = n$ water inflow period.

15

$$v^* = (A^*)^{0.5} / t_{end} \quad (15)$$

v^* : average overland flow velocity (mm/s) at the end of the water inflow period

Several parameters of the experimental plots which are usually estimated in overland flow studies (Smith et al., 2007) were also computed to ease comparisons of conditions in this study with reported data. As long as basic assumptions underlying their rationale are granted, the Froude number (**F**) relates the velocity of the overland laminar flow to the expected velocity of a gravitational wave, or the ratio of the laminar flow inertia to gravitational forces. Analogously, the dimensionless Reynolds number (**Re**) gives a measure of the ratio of inertial forces to viscous forces for given flow conditions. High Reynolds numbers characterize turbulent flow.

Statistical relations among measured and **F-Re** hydrodynamic variables (Eqs. 16-19) were identified through stepwise backward regressions analyses (SPSS 15.01, IBM Corporation, New York, USA).

4 Results

Figure 2 shows a comparison of the results obtained with the CRS-GSM procedure in a control plot where a DEM was also obtained through a regular optical-level/staff procedure.

A detailed analysis of these results is presented elsewhere (Rossi and Ares, 2012). It is here relevant to consider that local errors in the estimation of z values are in the millimetre range and although they are in cases related to singularities in the local micro-relief (small mounds, depressions), they are not systematic in this or in some other sense that could bias the results here presented.

Table 2 summarizes results obtained from the plot experiments. The upper vadose zone ($z_f \leq 55$ mm) of all plots showed various combinations of sand, silt and clay fractions within the boundaries of Sandy-Loam and Loamy-Sand USDA textural classes (Parameters 1-3) as well as their basic hydraulic properties (parameters 4-5, 9). The values of parameter 6 corresponded to very dry conditions of the upper soil due to the fact that all the plot experiments were performed during the dry season of the local climate regime. The range of water input flows (parameter 7) produced groups of fast and slow overland flow and water infiltration conditions. Model estimates of K_s at the upper vadose zone were significantly correlated to the ANN estimate based on textural data. The modeled time series of overland flow areas $A(t)$ (variable 10) were in all cases significantly correlated with the observed areas as indicated by the Nash-Sutcliffe's EC. At inter-plot level, parameters 11-16 were also significantly correlated with data values. $H_0: a = 0, b = 1$ was rejected in the case of parameter 16 ($z_{f,model} = -8.41 + 0.955 \times z_{f,data}$, $P = 1.42E-06$). This is to be expected due to the fact that $z_{f,data}$ were estimated from soil cores along the main overland flow axes, while $z_{f,model}$ expresses the average infiltration depth corresponding to the whole wet area. The model overall error in mass balance was in all cases $\leq 1 \times 10^{-7} \text{ mm}^3$.

No significant correlations were found between the extent of DS areas and other variables at the inter-plot scale. At intra-plot scale, DS areas at each time interval were (negatively) correlated (*: $P < 0.1$; **: $P < 0.05$) with the run-off coefficient ζ at plots under high water inflow (P1: -0.764**; P2: -0.767**; P3: -0.31; P4: -0.28) and in most cases was positively correlated with it at plots with low water inflow (P5: 0.243*; P6: 0.635**; P7: -0.799**; P8: 0.763**; P9: 0.656**; P10: 0.15).

Figure 3 shows four examples of the distribution of upper vadose zone (0-30 mm)

moisture ($\theta_{end, 0-30\text{ mm}}$) at four plots in this study. Depending on the position of the water inflow and the local microtopography, some areas contain moisture at near saturation levels while various levels of unsaturated conditions prevailed at other areas at the end of the water inflow period.

Figure 4 shows the comparison of z_f and θ_{end} values as obtained from the CHEMFLO-2000 simulation. These are compared with estimates from the model in section 3; photographs of soil cores at the water inflow areas are also shown for comparison.

Figure 5 shows $A(t)$ values of several plots as measured and estimated with the model of eq. (1)-(3). Table 3 summarizes theoretical hydrodynamic overland flow parameters of the plot experiments and the frictional parameter C obtained through inverse modelling of the system of Eqs. (1)-(3). Figure 6 shows statistical relations linking the variables in Table 3 including relations between C - F and d^* - Re . It is observed that C is significantly related to F and d^* is significantly related to Re , although their values are independent of the variations of flow rate across the plot series.

The analyses of the (standardized variables) results of all experiments further identify some significant statistical relations (***: $P < 0.01$) among plot characteristics:

$$C = (1.048 \times \gamma_{A/CW} - 0.156 \times \sigma_S + 0.114 \times S^*) \quad (r = 0.994^{***}) \quad (16)$$

$$\varsigma = (-0.439 \times C + 0.601 \times d^* + 0.794 \times W - 0.491 \times \log_{10} K_s) \quad (r = 0.958^{***}) \quad (17)$$

$$d^* = (-0.461 \times Re + 1.178 \times W) \quad (r = 0.946^{***}) \quad (18)$$

$$v^* = (1.039 \times W - 0.421 \times d^*) \quad (r = 0.995^{***}) \quad (19)$$

5 Discussion

5.1. On the experimental setup of this study. Implications in describing overland flows and infiltration in field conditions.

Plot studies on overland flows sometimes use natural rainfall falling on the plot as water input (Esteves et al., 2000) or a controlled water inflow either through rain simulation over the plot surface (Abrahams et al., 1990; Biemelt et al., 2005; Mügler et al., 2011), or through drippers, perforated pipes, etc. at the top of the plots (Dunkerley, 2001, 2003; Hessel et al., 2003). Further observation is performed on the characteristics (depth, flow velocity, run-off

discharge) of the resulting overland flow. Usually, plot studies also require some disturbance of naturally occurring conditions, like constructing flumes (Esteves et al., 2000; Giménez et al., 2004), modifying the soil surface to obtain desired flow channels (Mügler et al., 2011) or simulating the soil surface with technical artifacts (Dunkerley, 2003). Usual rainfall-run-off plot experiments may also require measuring the water flow at an outlet (Grierson and Oades, 1977; Cerdá et al., 1997). All these experimental setups may introduce artifacts affecting to some degree the characteristics of the overland flows as compared to those under field conditions.

In plot experiments where natural or simulated rain occurs over the plot area the kinetic energy of the rainfall may modify the overland flow momentum and velocity. Measured ranges of rainfall kinetic energy all over the world under various methods indicate a range of $12\text{--}22 \text{ J m}^{-2}\text{mm}^{-1}$ for a storm of 10 mm/h (Rosewell, 1986), which is a common event in semi-desert areas under tropical regime. Aside from potential effects on soil microtopography (erosion) these energy inputs can reasonably be expected to contribute to the overland flow momentum balance.

Flume plot experiments (Esteves et al., 2000; Dunkerley, 2004) may introduce various kinds of artifacts. To avoid wall effects, the soil relief must be manipulated in order to deliver the overland flow to the central part of the flume. In laboratory flume experiments, the natural soil must be transported and modifications in soil structure necessary follow. Overland flow studies using technical materials to simulate the soil surface might not reproduce field conditions.

Experiments on overland flow involving the measurement of run-off through an outlet (a need in computing water mass balances) may require modifications of the soil microtopography to deliver run-off to the outlet. Interflow measurement (Wang et al., 2011) might require sophisticated outlet configurations. The simultaneous occurrence of infiltration during the onset of overland flow introduces further complications to estimate flow characteristics. Locally varying infiltration rates introduce varying drags on overland flow kinetic energy because of mass removal from the flow.

Comparisons among results obtained in field studies on overland flows at various semi-arid/arid environments might benefit from biogeography analysis of the corresponding experimental sites. Regional similarities as estimated through comparative biogeography (Parenti and Ebach, 2009) result from analyzing spatial and functional patterns of biodiversity, species distribution, and geological history.

Some of the abovementioned potential limitations of plot studies on overland flow were avoided through the experimental setup of this study. Estimates of overland flow depth, velocity and friction were obtained without manipulation of the microtopography of field plots. Both overland flows and infiltration rates are considered simultaneously and the effect of depression storage areas on this latter is also estimated. The experimental results were tested through a physically based model of infiltration and surface friction. Possible extrapolation of the results to other similar desert areas is supported by the biogeography analysis of similarity (see section 2.1 above) of the environment where this study was performed with other desert areas of the world.

5.2. Effect of spatial variability of microtopography at plot scale on the infiltration-overland flow rates.

The consideration of the soil as a heterogeneous system at physical non-equilibrium (PNE) has been applied to a number of hydrological models (see Köhne et al., 2009 for an extensive review of various forms of published PNE models). In most cases, the emphasis has been focused on the effects of sub-surface soil heterogeneity on infiltration flows. In this study, attention is given to surface soil heterogeneity in the x - y plane and it is hypothesized that infiltration must occur under saturated conditions whenever DS occurs, while saturated-unsaturated infiltration could occur at non-DS areas. In considering this hypothesis, we introduce a complementary alternative to Antoine's et al. (2011) geometric interpretation of the DS concept by considering that depending on the rate of overland flow, unsaturated infiltration occurs at some areas of the soil where the water inflow is insufficient to maintain a free water film on the soil surface. This would hold whenever water infiltration rates in DS areas are high enough to keep pace with the local water supply rate. This interpretation is analogous to observations on composite overland flow by Abrahams et al. (1990) on run-off plots in arid southern Arizona (USA) where flow occurred as shallow sheets of water with threads of deeper, faster flow diverging and converging around surface protuberances, rocks, and vegetation.

The results here presented imply that the effect of DS areas on the overland flow velocity would be more complex than expected as areas of passive water storage. Saturated DS areas would be important for infiltration at high rates of water that would otherwise contribute to overland flow. This view is supported by the fact that the time serial correlation DS- ζ is negative or positive at plots with varying rates of water inflow. At plots P1-P4, (high

water input rates during short times), the saturated infiltration rate is negligible in comparison with the water inflow. In these cases, DS areas become filled before the underlying top soil reaches saturation and their behaviour would approach that of a passive impervious storage. This would result in run-off delay (negative DS- ζ correlation). In most of the cases where the water input occurs at low rates during longer periods (Plots P5-P10) DS areas become filled at a lower pace while the water input is nearly balanced by the high saturated conductivity at DS areas. After this period, infiltration in DS areas diminishes reaching a low, steady rate (Mao et al., 2008) and the run-off flow increases positively correlated with DS because no significant further infiltration at DS areas occurs. This would result in the observed predominantly positive DS- ζ correlations.

The results from the experimental plots are also consistent with those of Esteves et al. (2000), Parsons et al. (1990) and Parsons and Wainwright (2006) on the occurrence of composite flows during run-off-infiltration events. In the modelling experimentation during this study, it was not possible to simultaneously reproduce the observed values of overland flow areas $A(t)$ and the observed $\theta_{end} - z_f$ values unless saturated infiltration conditions were assumed in DS areas. Assuming saturated infiltration conditions over all the laminar flow area resulted in complete depletion of the overland water stock in all cases. This was contrary to the observed laminar flow expansions. Conversely, assuming unsaturated conditions over all the wetted soil area would not account for the observed $\theta_{end} - z_f$ values. A balance of saturated-unsaturated flows apportioned between DS and the rest of wet areas as estimated in this study yields results consistent with observations, as shown in Table 2.

5.3. Estimation of overland flow parameters

Equations (16- 19) show a set of statistical relations between characteristics of the infiltration-overland flow processes and parameters measured in the plot experiments here presented. The Darcy's formulation of a friction law in the form of Eq. (10) allows the estimation of the average overland flow depth d^* once the frictional term C is estimated through inverse modelling of the continuity Eqs. (1)-(3). C is equivalent to Chezy frictional constant except for replacing flow velocity through water inflow rate in Eq. (10). Values $d(t) - d^*$ obtained in this study are in a similar scale as those reported by Esteves et al. (2000) and instrumentally measured by Dunkerley (2001) in laboratory conditions and Smith et al. (2011) in field conditions.

The analysis of Eq (16) indicates that the meaning of C exceeds that of the strictly frictional term (σ_s) but also depends on the interaction of the ratio $\gamma_{A/W}$ and S^* . The former is a measure of the plot capacity to store infiltrated water at the upper vadose zone and the second is a measure of the effect of gravitational forces. Since infiltration introduces inertial drag on overland flow, Eq. (16) is (in a statistical sense) an empirical estimate of the ratio of inertial to gravity forces on the overland flow. This is further confirmed through the high correlation observed between C (frictional term) and the Froude number (Table 3b, Figure 6a). No significant correlations between C or Re and the Darcy-Weisbach's frictional coefficient f which is usually employed in overland flow modelling were observed.

Abrahams et al. (1990) working on sparsely vegetated desert hill slopes similar to those at our plots, observed that the relation of this coefficient with the Reynolds number varied during the inundation of roughness elements and the variations in overland flow depth.

Equations (17)-(19) allow computing the run-off coefficient ζ , the depth d^* and the overland flow velocity v^* from field and modelling data. The relation in Eq. (18)-Figure 6b deserves further attention, since the water kinematic viscosity involved in the computation of the Reynolds number changes by about 300% within inter-seasonal temperature ranges observable at the soil surface in the Patagonian Monte and similar areas with semi-arid/arid regime. This implies that estimates of d^* and resulting overland flows usual in hydrological practice in this type of environment should take account of seasonal temperature conditions at the site. This may probably apply to any modelling effort of overland flow processes that would need estimates of overland flow depth.

6. Conclusions

This study gives the following findings about the simultaneous occurrence of water infiltration and overland flow in conditions of arid regime at the Patagonian Monte: 1. Overland flow velocities as well as infiltration-overland flow mass balances are consistently modelled by considering variable infiltration rates corresponding to depression storage and/or non-ponded areas. 2. Several statistical relations are presented which can be used to estimate frictional C (Chezy's), run-off coefficient, average depth and velocity of overland flow under simultaneous infiltration in semi-arid/arid environments. A protocol of experiments in undisturbed field conditions and coupled time-distributed modelling to 1-2 above is described. A biogeography-based analysis of the experimental site is given to ease

comparisons with experiments on overland flows in other areas of the world.

Acknowledgements

This study was supported by grants of Agencia Nacional de Investigaciones Científicas y Técnicas (ANPCyT) PICT 07-1738 and Consejo Nacional de Investigaciones Científicas y Técnicas (CONICET) PIP 1142 0080 1002 01 to J. O. Ares. M. J. Rossi was a doctoral fellow from ANPCyT during 2009-2012.

References

- 10 Abraham, E., del Valle, H., Roig, F., Torres, L., Ares, J., Coronatp F., Godagnone R.: Overview of the geography of the Monte desert of Argentina. *Journal of Arid Environments* 73: 144-153, 2009.
- Abrahams, A.D., Parsons, A.J., and Luk, S.: Field experiments on the resistance to overland flow on desert hillslopes. *Erosion, Transport and Deposition Processes*, in: 15 *Proceedings of the Jerusalem Workshop, Jerusalem, March-April 1990, IAHS Publ. no. 189, 1990.*
- Aguilar, M.R., and Sala, O.E.: Patch structure, dynamics and implications for the functioning of arid ecosystems, *Trends in Ecology and Evolution*, 14, 273-277, 1999.
- Antoine, M., Chalon, C., Darboux, F., Javaux, M., and Biielders, C.: Estimating changes in 20 effective values of surface detention, depression storage and friction factor at the interrill scale, using a cheap and fast method to mold the soil surface microtopography, *Catena*, 91, 10-20, 2011.
- Ares, J.O., Beskow, M., Bertiller, M.B., Rostagno, C.M., Irisarri, M., Anchorena, J., Deffosé, G., and Merino, C.: Structural and dynamic characteristic of overgrazed grassland of 25 northern Patagonia, Argentina, in: *Managed Grassland*, Breymeyer, A., Elsevier Science, Amsterdam, 149-175, 1990.
- Ares, J.O., del Valle, H.F., and Bisigato, A.: Detection of process-related changes in plant patterns at extended spatial scales during early dryland desertification, *Glob. Change Biol.*, 9, 1643-1659, 2003.

- Bartley, R., Roth, C., Ludwig, J., McJannet, D., Liedloff, A., Corfield, J., Hawdon, A., and Abbott, B.: Runoff and erosion from Australia's tropical semi-arid rangelands: influence of ground cover for differing space and time scales, *Hydrol. Process.*, 20, 3317-3333, 2006.
- 5 Biemelt, D., Schappa, A., Kleeberg, A., and Grünewald, U.: Overland flow, erosion, and related phosphorus and iron fluxes at plot scale: a case study from a non-vegetated lignite mining dump in Lusatia, *Geoderma*, 129, 4-18, 2005.
- Borgogno, F., D'Odorico, P., Laio, F., and Ridolfi, L.: Mathematical models of vegetation pattern formation in ecohydrology, *Rev. Geophys.*, 47, 1–36, 2009.
- 10 Bromley, J., Brouwer, J., Barker, A.P., Gaze, S.R., and Valentin, C.: The role of surface water redistribution in an area of patterned vegetation in a semi-arid environment, south-west Niger, *J. Hydrol.*, 198, 1-29, 1997.
- Cammeraat, L. H.: A review of two strongly contrasting geomorphological systems within the context of scale, *Earth Surface Processes and Landforms*, 27, 1201-1222, 2002.
- 15 Carrera, A., Ares, J., Labraga, J., Thurner, S., and Bertiller, M.: Scenarios of Future Climate and Land-Management Effects on Carbon Stocks in Northern Patagonian Shrublands, *Environmental Management*, 40, 944–957, 2007.
- Carrera A. L., Bertiller, M. B. and Larreguy, C.: Leaf litterfall, fine-root production, and decomposition in shrublands with different canopy structure induced by grazing in the
20 Patagonian Monte, Argentina, *Plant Soil*, 311, 39-50, 2008.
- Cerdá, A., Ibáñez, S., and Calvo, A.: Design and operation of a small and portable rainfall simulator for rugged terrain, *Soil Technology*, 11, 163-170, 1997.
- Darboux, F., Davy, Ph., Gascuel-Oudou, C., and Huang, C.: Evolution of soil surface roughness and flowpath connectivity in overland flow experiments, *Catena*, 46, 125-
25 139, 2001.
- del Valle, H.F.: Patagonian soils: a regional synthesis, *Ecología Austral*, 8, 103–123, 1998.
- Descroix, L., Viramontes, D., Estrada, J., Gonzalez Barrios, J.L., and Asseline, J.: Investigating the spatial and temporal boundaries of Hortonian and Hewlettian runoff in Northern Mexico, *J. Hydrol.*, 346, 144-158, 2007.
- 30 Dingman, S.L.: Analytical derivation of at-a-station hydraulic–geometry relations, *J. Hydrol.*,

334, 17-27, 2007.

Dunkerley, D.L.: Estimating the mean speed of laminar overland flow using dye-injection-
Uncertainty on rough surfaces, *Earth Surf. Proc. Land*, 26, 363-374, 2001.

Dunkerley D.L.: Infiltration rates and soil moisture in a groved mulga community near Alice
5 Springs, arid central Australia: evidence for complex internal rainwater redistribution
in a runoff–runon landscape, *J. Arid Environ.*, 51, 199-219, 2002.

Dunkerley D.L.: Determining friction coefficients for interrill flows. The significance of flow
filaments for interrill flows, *Earth Surf. Process. Landforms*, 28, 475–491, 2003.

Dunkerley, D.L.: Flow threads in surface run-off: implications for the assessment of flow
10 properties and friction coefficients in soil erosion and hydraulics investigations, *Earth
Surf. Proc. Land.*, 29, 1011–1026, 2004.

Esteves, M., Faucher, X., Galle, S., and Vauclin, M.: Overland flow and infiltration
modelling for small plots during unsteady rain: numerical results versus observed
values, *J. Hydrol.*, 228, 265-282, 2000.

15 Ewen, J.: Hydrograph matching method for measuring model performance, *J. Hydrol.*, 408,
178-187, 2011.

Gee, G.W., and Bauder J.W.: Particle-size analysis, in: Klute, A. (Ed.), *Methods of soil
analysis. Part 1. Physical and mineralogical methods*, 2.ed., Madison: ASA-SSSA.
Agronomy Monograph No. 9. pp. 383-411, 1986.

20 Giménez, R., Planchon, O., Silvera, N., and Govers, G.: Longitudinal velocity patterns and
bed morphology interaction in a rill, *Earth Surf. Proc. Land.*, 29, 105–114, 2004.

Govers, G., Takken, I., and Helming, K.: Soil roughness and overland flow, *Agronomie*, 20,
131-146, 2000.

Gowdish, L., and Muñoz-Cárpena, R.: An Improved Green–Ampt Infiltration and
25 Redistribution Method for Uneven Multistorm Series, *Vadose Zone J.*, 8, 470-479,
2009.

Green, W.H., and Ampt, G.A.: Studies on soil physics: 1. the flow of air and water through
the soils, *J. Agr. Sci.*, 4, 1-24, 1911.

Grierson, I.T., and Oades, J.M. A rainfall simulator for field studies of run-off and soil
30 erosion. *J. Agr. Eng. Research*, 22, 37-44, 1977.

- Hansen, B.: Estimation of surface runoff and water-covered area during filling of surface micro relief depressions, *Hydrol. Process.*, 14, 1235-1243, 2000.
- Haylock, M.R., Petersen, T.C., Alves, L.M. et al.: Trends in total and extreme South American rainfall in 1960-2000 and links with sea surface temperature, *J. Climate*, 5 19, 1490-1512, 2006.
- Hessel, R., Jetten, V., and Guanhui, Z.: Estimating Manning's n for steep slopes, *Catena*, 54, 77-91, 2003.
- Köhne, J.M., Köhne, S., and Simunek, J.: A review of model applications for structured soils: a) water flow and tracer transport, *J. Contam. Hydrol.*, 104, 4-35, 2009.
- 10 Latron, J., and Gallart, F.: Seasonal dynamics of runoff-contributing areas in a small Mediterranean research catchment (Vallcebre, Eastern Pyrenees), *J. Hydrol.*, 335, 194–206, 2007.
- Legout, C., Darboux, F., Nédélec, Y., Hauet, A., Esteves, M., Renaux, B., Denis, H., and Cordier S.: High spatial resolution mapping of surface velocities and depths for 15 shallow overland flow, *Earth Surf. Proc. Land.*, DOI 10.1002/esp.3220.
- León, R.J.C., Bran, D., Collantes, M., Paruelo, J.M., and Soriano, A.: Grandes unidades de vegetación de la Patagonia extraandina, *Ecología Austral*, 8, 125-144, 1998.
- Li, G.: Preliminary study of the interference of surface objects and rainfall in overland flow resistance, *Catena*, 78, 154-158, 2009.
- 20 Li, X., Contreras, S., Solé-Benet, A., Cantón, Y., Domingo, F., Lázaro, R., Lin, H., Van Wesemael, B., and Puigdefábregas, J.: Controls of infiltration–runoff processes in Mediterranean karst rangelands in SE Spain, *Catena*, 86, 98-109, 2011.
- Lipsius, K., and Mooney, S.J.: Using image analysis of tracer staining to examine the infiltration patterns in a water repellent contaminated sandy soil, *Geoderma*, 136, 865- 25 875, 2006.
- Mao, L.L., Lei, T.W., Li, X., Liu, H., Huang, X.F., and Zhang, Y.N.: A linear source method for soil infiltrability measurement and model representations, *J. Hydrol.*, 353, 49-58, 2008.

- Mares, M.A., Morello, J. and Goldstein, G.: Semi-arid shrublands of the world, chapter 10 in: Hot deserts and arid shrublands. Ecosystems of the world, Evenari, M., Noy-Meir, I., and Goodall, D., Elsevier, Amsterdam, The Netherlands, 203–237, 1985.
- 5 Mengistu, B., Defersha, A., and Melesse, M.: Field-scale investigation of the effect of land use on sediment yield and runoff using runoff plot data and models in the Mara River basin, Kenya, *Catena*, 89, 54-64, 2012.
- Morello, J.H.: Perfil Ecológico de Sud América. Instituto de Cooperación Iberoamericana. 1984, 30 pp.
- 10 Mualem, Y.: A new model for predicting the hydraulic conductivity of unsaturated porous media, *Water Resour. Res.*, 12, 593-622, 1976.
- Muñoz-Cárpena, R., and Gowdsh, L.: Aplicación del método de infiltración de Green-Ampt con redistribución de humedad del suelo entre encharcamientos, in: Estudios de la Zona no-saturada del suelo vo. VII., Samper, F., Calvete, J., and Paz Gonzalez, A., La Coruña, 205-213, 2005.
- 15 Mügler, C., Planchon, O., Patin, J., Weill, S., Silvera, N., Richard, P., and Mouche, E.: Comparison of roughness models to simulate overland flow and tracer transport experiments under simulated rainfall at plot scale, *J. Hydrol.*, 402, 25-40, 2011.
- Nash, J.E., and Sutcliffe, J.V.: River flow forecasting through conceptual models, 1, a discussion of principles, *J. Hydrol.*, 10, 282-290, 1970.
- 20 Nofziger, D.L., and Wu, J.: CHEMFLO-2000. Interactive Software for Simulating Water and Chemical Movement in Unsaturated Soils, Department of Plant and Soil Sciences Oklahoma State University Stillwater, Oklahoma, 2003.
- Parenti, L.R., and Ebach, M.C.: Comparative Biogeography. Univ. of California Press, Princeton, 312 pp., 2009.
- 25 Parsons, A.J., Abrahams, A.D., and Luk, S.H.: Hydraulics of interrill overland flow on a semi-arid hillslope, southern Arizona, *J. Hydrol.*, 117, 255-273, 1990.
- Parsons, A.J., Wainwright, J. :Depth distribution of interrill overland flow and the formation of rills. *Hydrological Processes*, 20 , 1511-1523, 2006.
- 30 Planchon, O., and Darboux, F.: A fast, simple and versatile algorithm to fill the depressions of digital elevation models, *Catena*, 46, 159-176, 2002.

- Prohaska, F.: The climate of Argentina, Paraguay and Uruguay, in: W. Schverdtfeger (Ed.), Ch. 2, pp. 13-112, *Climates of Central and South America*, Elsevier, Amsterdam, 532 pp., 1976.
- Radcliffe D.R., and Simunek, J.: *Soil Physics with HYDRUS: Modeling and Applications*,
5 CRC Press, New York, 2010.
- Reaney, S.M.: The use of agent based modelling techniques in hydrology: determining the spatial and temporal origin of channel flow in semi-arid catchments, *Earth Surf. Proc. Land*, 33, 317-327, 2008.
- Rosewell, C.J.: Rainfall kinetic energy in Eastern Australia, *J. Climate Appl. Meteorology*,
10 25, 1695-1701, 1986.
- Rossi, M.J., and Ares J.O.: Close range stereo-photogrammetry and video imagery analyses in soil eco-hydrology modelling, *Photogrammetric Record*, 27, 111-126, 2012.
- Schaap, M.G., and Leij, F.J.: Database Related Accuracy and Uncertainty of Pedotransfer Functions, *Soil Sci.*, 163, 765-779, 1998.
- 15 Schröder, A.: WEPP, EUROSEM, E-2D results of application at the plot scale, in: *Soil Erosion-Application of Physically Based Models*, Schmidt, J., Berlin, Heidelberg, New York, 199-250, 2000.
- Smith, M.W., Cox, N.J., and Bracken, L.J.: Applying flow resistance equations to overland flows, *Prog. Phys. Geog.*, 31, 363-387, 2007.
- 20 Smith, M. W., Cox, N. J., Bracken, L. J. Modeling depth distribution of overland flows. *Geomorphology*, 125, 402-413, 2011.
- Soriano, A.: La vegetación del Chubut, *Revista Argentina de Agronomía*, 17, 30–66, 1950.
- Tarboton D.G., and Ames D.P.: Advances in the mapping of flow networks from digital elevation data, *World Water and Environmental Resources Congress*, Orlando,
25 Florida, 20-24 May, ASCE, 2001.
- Tatard, L., Planchon, O., Wainwright, G., Nord, J., Favis-Mortlock, D., Silvera, N., Ribolzi, O., Esteves, M., and Huang C.H.: Measurement and modelling of high-resolution flow-velocity data under simulated rainfall on a low-slope sandy soil, *J. Hydrol.*, 348, 1–12, 2008.
- 30 Thompson, S., Katul, G., Konings, A., and Ridolfi, L.: Unsteady overland flow on flat

surfaces induced by spatial permeability contrasts, *Adv. Water Resour.*, 34, 1049-1058, 2011.

van Genuchten, M.Th.: A closed form equation for predicting the hydraulic conductivity of unsaturated soils, *Soil Sci. Soc. Am. J.*, 44, 892-898, 1980.

5 van Schaik, N.L.: Spatial variability of infiltration patterns related to site characteristics in a semi-arid watershed, *Catena*, 78, 36-47, 2009.

Wang, J., Yang, H., Li, L., Gourley, J. Sadiq, K. et al.: The coupled routing and excess storage distributed hydrological model, *Hydr. Sci. J.*, 56, 84-98, 2011.

10 Weill, S., Mazzia, A., Putti, M., and Paniconi, C.: Coupling water flow and solute transport into a physically-based surface–subsurface hydrological model, *Adv. Water Resour.*, 34, 128-136, 2011.

15

20

Table 1. Parameters and variables of soil surface and upper vadose and convergence criteria used in validating a model of the field plot experiments. ANN CI: Confidence interval of the ANN estimation process; r : correlation coefficient, linear regression model-data values ($x_{model} = a + b \times x_{data}$; $H_0: a = 0, b = 1$) over all plot experiments. ($A(t)$): convergence evaluated at 10-15 times during the water inflow period. (***: statistical significance at $P < 0.01$)

	Parameter	Convergence criteria	Compartment
1	Sand (%)	Data value	Soil
2	Silt (%)	Data value	Soil
3	Clay (%)	Data value	Soil
4	θ_{sat}	Data value	Soil
5	θ_r	Data value	Soil
6	$\theta_{antecedent}$	Data value	Soil
7	Water inflow W (mm ³ /s)	Data value	Surf. soil
8	Water inflow period (s)	Data value	Surf. soil
9	K_s (mm/s)	ANN CI - r (**)	Soil
10	Wet Area ($A(t)$)(mm ²)	EC ≥ 0.99 ^a	Surf. soil
11	Total Wet Area (A^*) (mm ²)	r (***)	Surf. soil
12	Average run-off velocity (mm/s)	r (***)	Surf. soil
13	Average S (mm)	r (***)	Surf. soil
14	Average DS area (%)	r (***)	Surf. soil
15	θ_{end}	r (***)	Soil
16	z_f (mm)	r (***)	Soil
17	Water mass balance error (mm ³)	$e < 1E-6$ mm ³	Soil

^a Nash and Sutcliffe, 1970.

Table 2. Experimental results and model parameter values.

Parameter, variable		P1	P2	P3	P4	P5	Plots P6	P7	P8	P9	P10	<i>r</i>	<i>CI</i> ^a
1	Sand (%)	80.7	80.8	74.2	71.2	68.4	76.2	70.4	65.5	73.6	76.8		
2	Silt (%)	12.0	10.3	13.8	14.4	14.9	17.3	15.6	20.1	10.4	10.4		
3	Clay (%)	7.3	9.2	12.0	14.4	16.7	6.5	14.0	14.4	16.0	12.8		
4	θ_{sat}	0.38	0.38	0.39	0.38	0.38	0.39	0.38	0.38	0.38	0.38		
5	θ_r	0.04	0.05	0.05	0.05	0.04	0.04	0.05	0.05	0.05	0.05		
6	$\theta_{antecedent}$	0.06	0.05	0.06	0.11	0.05	0.04	0.05	0.05	0.06	0.06		
7	Water inflow W (mm ³ /s)	4500	4500	4500	4500	308	442	450	408	500	225		
8	Water inflow period (s)	72	96	48	72	1128	1026	714	660	792	852		
9	K_s (mm/s)	<i>1.1E-02</i>	<i>1.1E-02</i>	<i>8.2E-03</i>	<i>5.8E-03</i>	<i>5.3E-03</i>	<i>9.2E-03</i>	<i>1.2E-03</i>	<i>2.9E-03</i>	<i>4.5E-03</i>	<i>6.5E-03</i>	<i>0.865</i>	<i>9.0E-02</i>
		1.1E-02	9.7E-03	5.7E-03	4.7E-03	6.2E-03	8.2E-03	4.2E-03	3.6E-03	4.4E-03	5.9E-03		
10	Wet Area ($A(t)$) (mm ²)	<i>0.996</i> ^b	<i>0.994</i>	<i>0.996</i>	<i>0.997</i>	<i>0.990</i>	<i>0.990</i>	<i>0.994</i>	<i>0.995</i>	<i>0.999</i>	<i>0.998</i>		
11	Total Wet Area (A^*) (mm ²)	<i>1.6E+05</i>	<i>3.7E+04</i>	<i>5.2E+04</i>	<i>1.4E+05</i>	<i>5.3E+04</i>	<i>5.4E+04</i>	<i>1.1E+05</i>	<i>7.4E+04</i>	<i>7.3E+04</i>	<i>3.2E+04</i>	<i>0.999</i>	<i>2.5E-04</i>
		1.6E+05	3.6E+04	5.1E+04	1.4E+05	5.5E+04	5.3E+04	1.1E+05	7.5E+04	7.3E+04	3.2E+04		
12	Average run-off velocity (mm/s)	<i>5.55</i>	<i>1.96</i>	<i>4.77</i>	<i>5.24</i>	<i>0.20</i>	<i>0.23</i>	<i>0.47</i>	<i>0.41</i>	<i>0.34</i>	<i>0.21</i>	<i>0.999</i>	<i>1.7E-04</i>
		5.56	1.98	4.73	5.25	0.21	0.22	0.47	0.42	0.34	0.21		
13	Average S (mm)	<i>0.3</i>	<i>1.8</i>	<i>4.5</i>	<i>1.8</i>	<i>1.2</i>	<i>2.7</i>	<i>0.5</i>	<i>1.0</i>	<i>2.1</i>	<i>0.3</i>	<i>0.971</i>	<i>2.5E-02</i>
		0.2	1.6	4.6	1.5	1.5	3.4	0.7	1.0	1.8	0.3		
14	Average DS area (%)	<i>9.1</i>	<i>2.7</i>	<i>2.9</i>	<i>2.7</i>	<i>4.7</i>	<i>7.6</i>	<i>7.3</i>	<i>1.0</i>	<i>10.1</i>	<i>14.7</i>	<i>0.941</i>	<i>2.2E-02</i>
		11.1	1.4	2.9	1.5	5.2	6.4	9.3	1.5	10.0	12.3		
15	θ_{end}	<i>0.19</i>	<i>0.21</i>	<i>0.19</i>	<i>0.2</i>	<i>0.18</i>	<i>0.2</i>	<i>0.13</i>	<i>0.13</i>	<i>0.19</i>	<i>0.17</i>	<i>0.985</i>	<i>2.2E-02</i>
		0.19	0.21	0.19	0.2	0.18	0.20	0.13	0.12	0.20	0.17		
16	z_f (mm)	<i>14</i>	<i>12</i>	<i>13.5</i>	<i>12</i>	<i>36</i>	<i>43</i>	<i>24</i>	<i>35</i>	<i>34</i>	<i>42</i>	<i>0.968</i>	<i>1.6E-02</i>
		23	21	24	27	47	53	28	42	45	55		
17	Water mass balance error (mm ³)	<i>6.E-11</i>	<i>-1.E-09</i>	<i>2.E-10</i>	<i>2.E-10</i>	<i>-1.E-07</i>	<i>6.E-10</i>	<i>6.E-10</i>	<i>2.E-10</i>	<i>-3.E-10</i>	<i>-3.E-10</i>		

All model estimates in bold italics.

^a Confidence interval (**) of the mean of 5 random samples out of 10 values.

^b Nash-Sutcliffe's Efficiency Coefficient (see also Figure 5).

Table 3. Froude (**F**), Reynolds (**Re**), Friction (Darcy-Weisbach's f) numbers and C , d^* parameter values of the field plot experiments.

a

		P1	P2	P3	P4	P5	P6	P7	P8	P9	P10
1	F ^a	0.102	0.006	0.033	0.064	0.001	0.001	0.004	0.006	0.003	0.002
2	Re ^b	7.407	101.775	45.758	16.217	2.186	3.715	2.582	0.840	1.726	1.098
3	f ^c	4.96E-01	2.85E+03	1.48E+02	8.95E+00	2.40E+04	6.55E+04	7.11E+02	9.10E+02	6.19E+03	3.10E+03
4	C	1.05E+05	4.80E+03	7.60E+03	2.90E+04	1.00E+03	8.60E+02	3.80E+03	3.50E+03	2.00E+03	2.70E+03
5	d^*	0.300	11.400	2.160	0.690	2.410	3.700	1.250	0.480	1.150	1.170

^a $F = v / (g \times d^*)^{0.5}$; $g = 9806.65 \text{ mm/s}^2$

^b $Re = 4 \times v^* \times d^* / \nu$; $\nu = 0.9 \text{ mm}^2/\text{s}$

^c $f = 8 \times g \times d^* / S^*$

b **Correlation table**

	F	Re	f	C	d^*
F	1.00				
Re	-0.01	1.00			
f	-0.33	-0.21	1.00		
C	0.93	-0.09	-0.25	1.00	
d^*	-0.31	0.88	0.15	-0.27	1.00

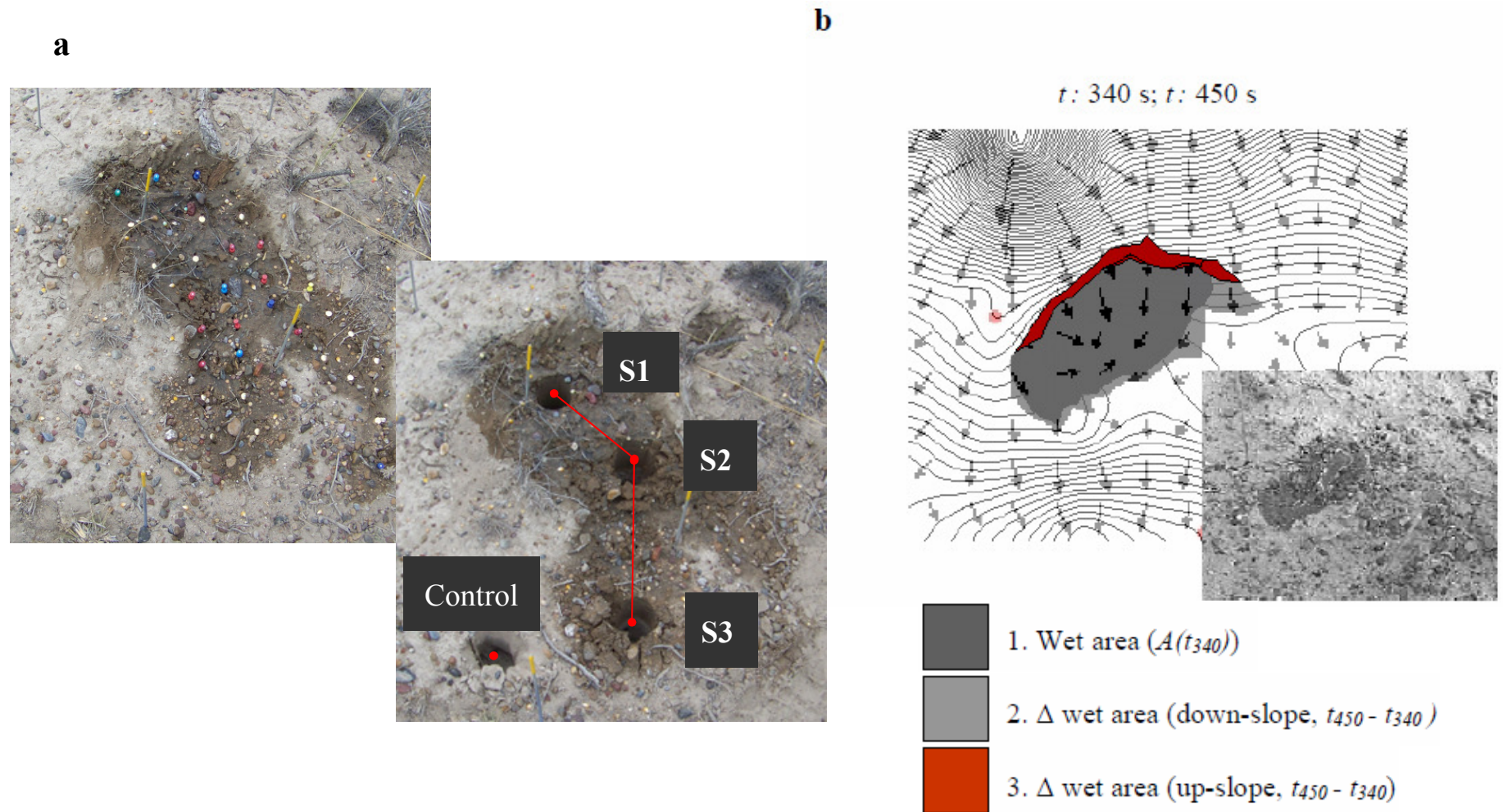


Fig. 1. (a) (Left) Overhead view of field plot at the end of the water inflow period with TDR probe position marks. **(Right)** Soil cores along the main axis of the overland flow area are already extracted. Flow occurred from S1 to S3. Spikes with control marks for CRS-GSM are shown. **(b)** Example (Plot #10) of the procedure used to estimate the progression of Depression Storage (DS) areas. Video scenes (lower-right inset) obtained at times 340 s and 450 s after water inflow start were overlaid on the plot DEM (contour interval: 1 mm shown) and flow arrows (rate of flow proportional to arrow length). Sectors where the overland flow advances against local up-slope are considered DS areas.

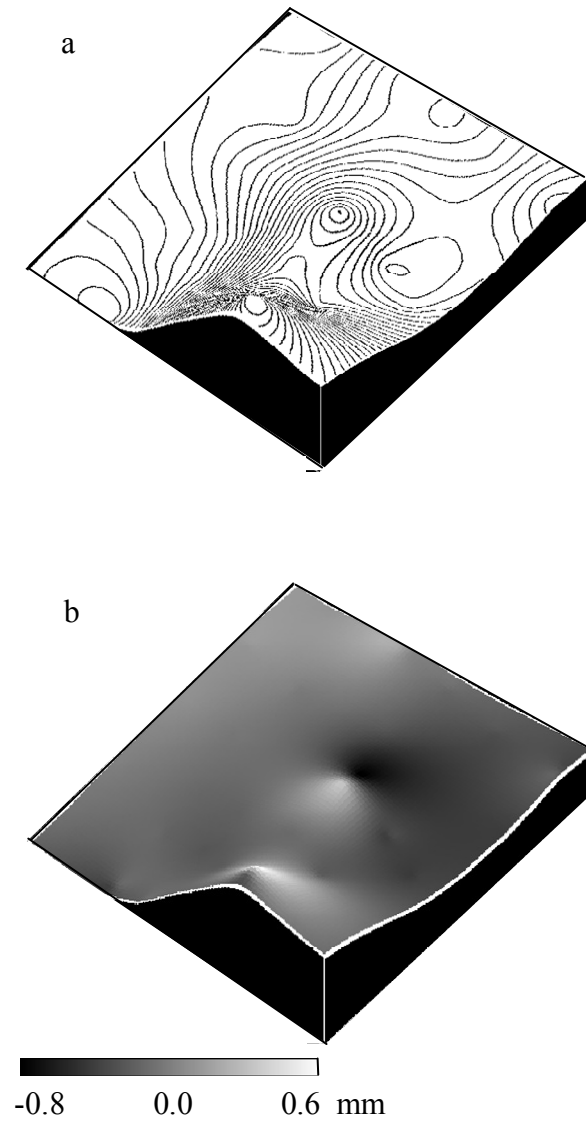


Fig. 2. (a) 3-D view of a plot DEM of 800×800mm with draped height contours (interval: 1.5 mm, maximum height $z = 77\text{mm}$) obtained with the close-range photogrammetry procedure used in this study. **(b)** 3-D view of the same DEM with draped image of the spatial distribution of the standard error in z estimates, respect the value obtained with optical level-topography staff method.

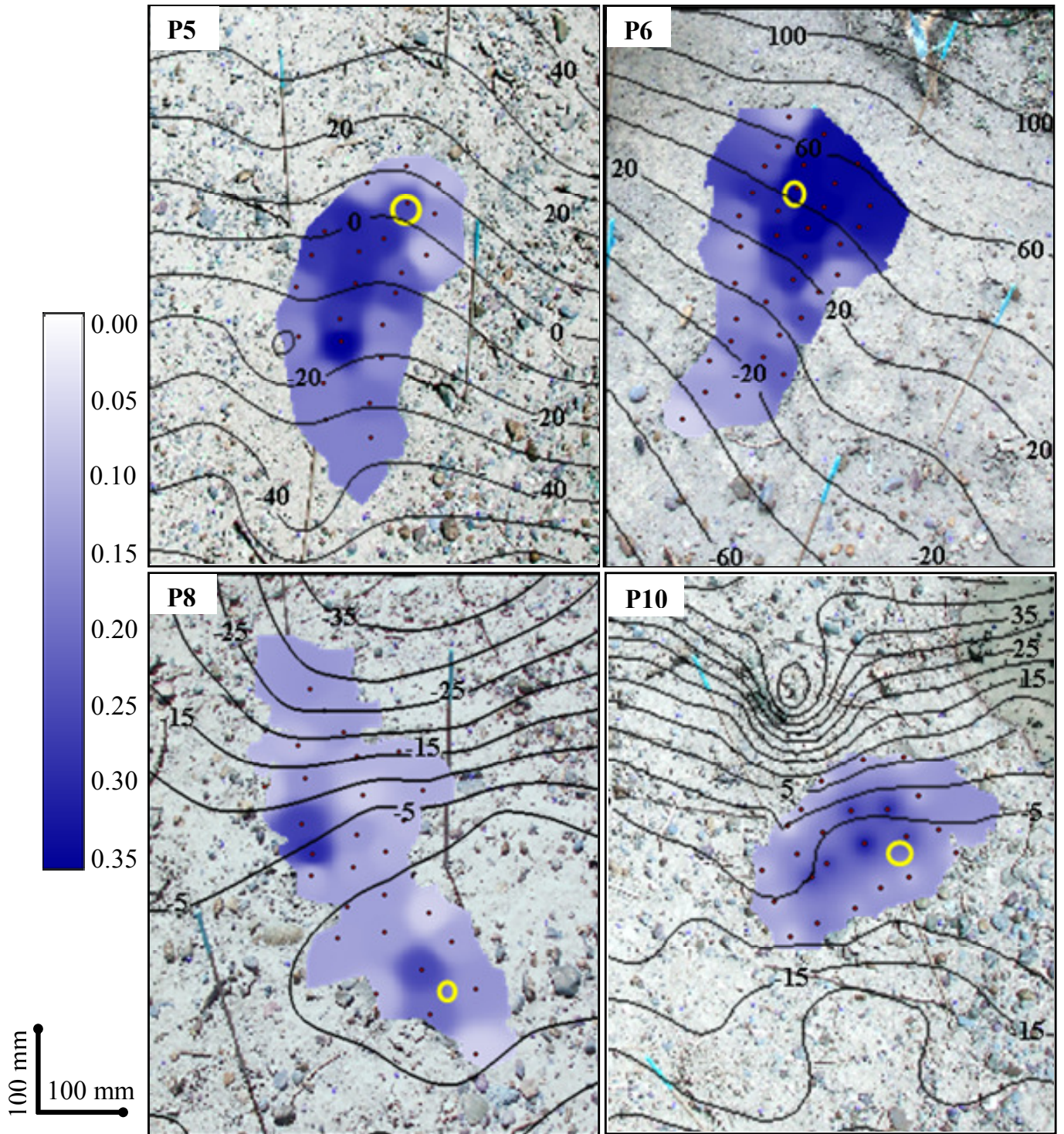


Fig. 3. Upper soil moisture ($\theta_{end, 0-30mm}$) maps of the overland plumes based on TDR probing (red dots) at the end of the water inflow periods at four plots in this study. Yellow circles indicate the water inflow areas. Maps overlay rectified plot photos and corresponding level (mm) contour lines.

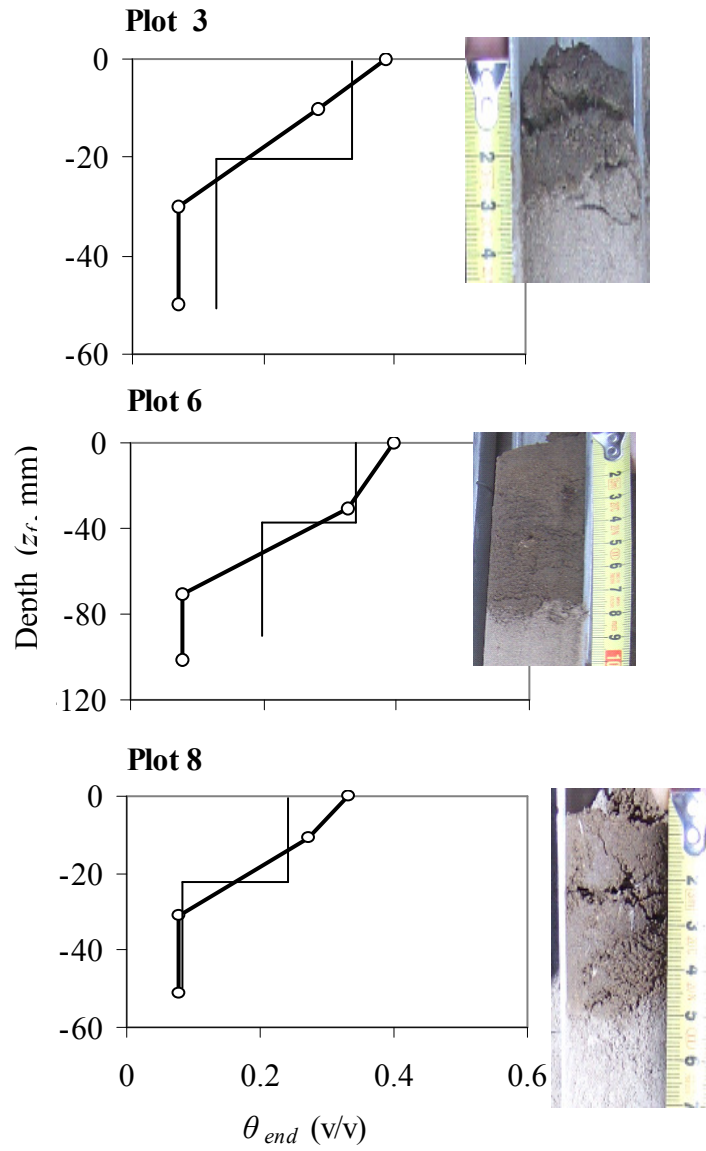


Fig. 4. Comparison of z_f (photo insets) and θ_{end} field soil core data (circle-lines) used as input the model in this study and estimates through CHEMFLO-2000 (lines). Soil core photos obtained immediately after ceasing water inflow are also shown.

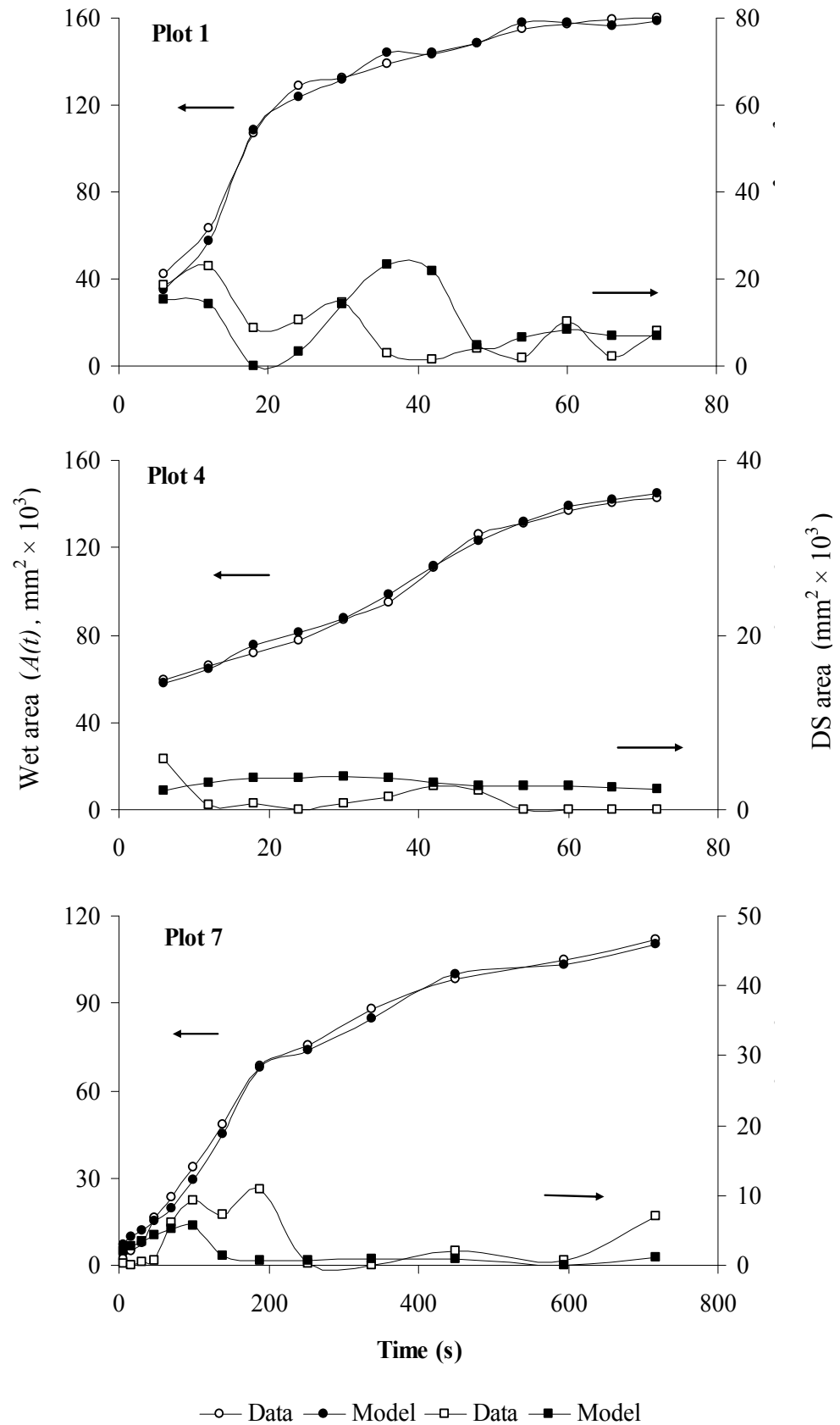


Fig. 5. The progression of overland flow $A(t)$ and DS areas during the water inflow periods in three field plots as estimated from rectified video imagery and the model used in this study.

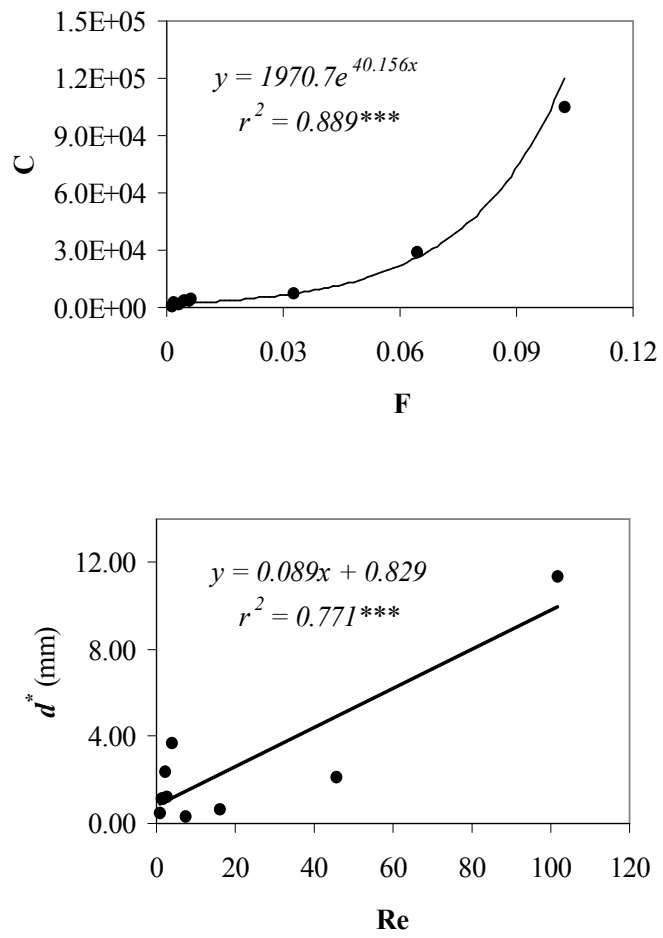


Fig. 6. Inter-plot statistical relations between parameters C - F and d^* - Re (***: $P < 0.01$)